

International Journal of Hydromechatronics

ISSN online: 2515-0472 - ISSN print: 2515-0464

<https://www.inderscience.com/ijhm>

CFD-based method for hydrostatic bearings performance: static characteristics with various recess shapes

Minghui Guo, Zhuxin Tian, Xiaolin Feng, Yu Huang, Guojun Zhang, Youmin Rong

DOI: [10.1504/IJHM.2024.10063433](https://doi.org/10.1504/IJHM.2024.10063433)

Article History:

Received:	22 July 2023
Last revised:	08 November 2023
Accepted:	28 November 2023
Published online:	30 April 2024

CFD-based method for hydrostatic bearings performance: static characteristics with various recess shapes

Minghui Guo

State Key Lab of Digital Manufacturing Equipment and Technology,
School of Mechanical Science and Engineering,
Huazhong University of Science and Technology,
Wuhan, 430074, China
Email: guomh@hust.edu.cn

Zhuxin Tian

College of Mechanics and Power Engineering,
China Three Gorges University,
Yichang, 443002, China
Email: zhuxintian1987@sina.com

Xiaolin Feng

Faculty of Engineering and Life Sciences,
Universiti Selangor,
Bestari Jaya, Selangor,
45600, Malaysia
Email: 1280060810@qq.com

Yu Huang, Guojun Zhang and Youmin Rong*

State Key Lab of Digital Manufacturing Equipment and Technology,
School of Mechanical Science and Engineering,
Huazhong University of Science and Technology,
Wuhan, 430074, China
Email: yuhuang_hust@hust.edu.cn
Email: zgj@hust.edu.cn
Email: rym@hust.edu.cn

*Corresponding author

Abstract: Hydrostatic bearings with recess are vulnerable to non-uniform oil film pressure and area effects. The above situation leads to decrease in stability and load carrying capacity (LCC) of bearings. In this paper, the influence of oil recesses structure on hydrostatic thrust bearings performance is discussed. The six oil recesses shapes were selected, and the static characteristics of bearings were simulated by using CFD method. The obtained results show that there are many differences in static characteristics of the hydrostatic thrust bearing caused by different recess shapes. The LCC increases with the recess circumference, and the maximum on equilateral triangle recess. It decreased

16.46% when the rotation speed from 0 to 5,000 rpm. The recess shape has no significant influence on the temperature distribution of oil film, but the average temperature is inversely proportional to the width of middle circle. Experiments are carried out to validate the simulations. When the bearing rotate speed at 1,000 rpm, the difference between experimental and simulation remains within 5%, indicating the validation of the CFD method.

Keywords: hydrostatic bearings; recess shape; CFD method; static characteristics.

Reference to this paper should be made as follows: Guo, M., Tian, Z., Feng, X., Huang, Y., Zhang, G. and Rong, Y. (2024) 'CFD-based method for hydrostatic bearings performance: static characteristics with various recess shapes', *Int. J. Hydromechanics*, Vol. 7, No. 2, pp.176–192.

Biographical notes: Minghui Guo received her MS in Mechanical Engineering from Northeast Forestry University, Harbin, China in 2018. She is currently pursuing her PhD in Mechanical Engineering Huazhong University of Science and Technology. Her research interests in textured and hydrostatic bearings.

Zhuxin Tian received his Bachelor in Mechanical Design Manufacturing and Automation in 2009 from Huazhong University of Science and Technology, Wuhan, China. He has obtained his PhD in Mechatronic Engineering from Huazhong University of Science and Technology in 2018. After then, he joined Hubei University of Arts and Science as a Lecturer. His research interests include hydrostatic and hydrodynamic bearings.

Xiaolin Feng received his Bachelor and MS in Mechanical Engineering from Northeast Forestry University. He is currently pursuing his PhD in Faculty of Engineering and Life Sciences, Universiti Selangor, Selangor, Malaysia. His research interests include hydrostatic and hydrodynamic bearings.

Yu Huang received his MS and PhD in Automotive Engineering and Mechanical Design Manufacturing and Automation from Huazhong University of Science and Technology in 2000 and 2004, respectively. After then, he joined Huazhong University of Science and Technology as a Lecturer. His current position is a Professor and the Deputy Director of the National engineering research centre for digitalisation of manufacturing equipment. His research areas cover high performance hydrostatic bearing, laser fine processing technology and equipment and high-power laser cutting and welding equipment.

Guojun Zhang received his PhD in Automotive Engineering and Mechanical Design Manufacturing and Automation from Huazhong University of Science and Technology. After then, he joined Huazhong University of Science and Technology as a Lecturer. His current position is a Professor and the research areas cover automatic control, ultra-precision machining, etc.

Youmin Rong received his PhD in Automotive Engineering and Mechanical Design Manufacturing and Automation from Huazhong University of Science and Technology. After then, he joined Huazhong University of Science and Technology as a Lecturer. His current position is an Associate Professor and research area includes ultra-precision machining, laser welding, etc.

1 Introduction

Hydrostatic bearings are widely used in precision machine tools for precision grinding of complex aerospace parts, precision turning for the engineering industry and medical equipment manufacturing (Li et al., 2022; Liu and Yang, 2022), etc. This is because the advantages of hydrostatic bearings such as high load carrying capacity (LCC), near zero friction, no wear, high efficiency, smooth movement and effective isolation from vibration transmission during operation (Xue et al., 2018). The recess such as the number, size and shape are the key position in the hydraulic circuit supply of the liquid hydrostatic bearing, ensured the pressure of the oil film is evenly distributed by recess with loading applied. Dynamic and static bearing characteristics are influenced by the structure of recess (Michalec et al., 2021), and using new forms of recess structure can improve oil film stiffness, dynamic pressure effect and vibration resistance. The bearing oil recess area provides sufficient lifting force for the bearing load. hydrostatic bearings with oil recess can withstand higher rotating speeds and load variations (Yacout et al., 2006; Yacout, 2007; Liu and Lu, 2022). Over the last few decades, many researchers had discussed the dynamic and static characteristics hydrostatic bearing with oil recess. However, hydrostatic bearings with oil recess are susceptible to oil film pressure instability and area effects on LCC, especially under the condition of various geometrical oil recess shapes (Dong et al., 2020). The influence of oil recess shape on the performance characteristics of hydrostatic bearings need to be investigate. It is critically important for the design and manufacture of high-performance and stable hydrostatic spindles.

For hydrostatic bearings, different oil recess shapes exhibit slightly different characteristics. The Reynolds equation is solved to calculate the temperature, pressure distribution and LCC with different oil recess configurations. Due to the linear solution and manufacturing methods, most preferred recess shapes are the circular, rectangular and ring-shaped conventional ones (Sharma et al., 2022). Recess three-dimensional shapes also have an influence on the static characteristics of hydrostatic bearings, such as Sharma et al. (Kumar and Sharma, 2017, 2019; Kumar et al., 2020) used finite element method to solve the Reynolds equation and calculated the performance of a single-recess thrust bearing as a function of recess geometry, the highest load carry capacity is in the annular oil recess. And in porous hydrostatic bearings, circular and square recess should be preferred because they provide better stiffness and damping capacity. Shen et al. (2014) conducted numerical calculation and experiment on various shapes of recess thrust bearings, they concluded that the highest maximum pressure in annular recess and the highest oil film stiffness in circular recess. Yu et al. (2019) and Zhang et al. (2010) used finite volume method analysis, determined the optimum shape recess performance under high speed and heavy load conditions. Yadav et al. (Saurabh et al., 2014) considered combined tilt and recess shape on the performance of hydrostatic thrust bearings, results showed the tilt angle was significant effect while the shape not. Untaroiu and Fu (2017) adjusted the design variables to maximise load capacity while minimising bearing power loss from friction torque. Sing et al. (2004) solved the controlling equations for lubricant flow, the three-dimensional elasticity equations and the throttle flow equations by using the finite element method, investigated the triangular shape provide the highest film thickness. Dzodzo et al. (1996) calculated the effect of oil recess edge on bearing performance, the square corners provided higher recess pressure, the

rounded corners created a smoother profile to maintain better flow of pressurised fluid and dissipate heat.

Although the different shaped oil recess on hydrostatic bearings were analysed in the above research, and most results have focused on circular and annular oil recesses. The bearings with rectangular oil recess (Zhang et al., 2018) and sector oil recess (Xu et al., 2013) were also investigated by other researchers. At the same time, most research has concentrated on single-pad hydrostatic bearings while little research into the multi-recess bearings. In engineering applications, multi-recess hydrostatic bearings are more used in high speed spindles due to low oil film pressure fluctuations, high accuracy and stability (Kozdera and Drbáková, 2013; Shaaban, 2022; Yu et al., 2015). In addition, the performance of the above bearings was investigated under static conditions. Under the rotating state, little attention has been paid to the influence of the recess shape on the performance behaviour of the bearing, especially at high speeds. The temperature of the oil film is an important factor must be considered over 3,000 rpm. The high-speed hydrostatic bearings are becoming very important for micro-grinding and electronic manufacturing under the large load.

Here, an investigation of hydrostatic thrust bearings static characteristics on six different shapes recess is discussed. Numerical simulation models with different recess shapes were established based on the CFD method. In the bearing boundary conditions, the coefficient of lubricant viscosity-temperature was derived. And the user-defined function (UDF) was used to define the coefficient. The static characteristics of different shapes recess bearing such as pressure distributions, LCC and temperature were investigated under various operating conditions. The lubricant flow characteristics and the oil film temperature heat transfer properties were cover in the operational conditions. Finally, experimental tests were carried out on the constructed test rig to verify the validity of CFD method.

2 Model and finite volume method

2.1 Three-dimensional model and mesh

The model of hydrostatic thrust bearing as shown in Figure 1. The thrust bearing tested was a fixed geometry planar bearing comprising six pads (flat lands parallel to the runner surface). Each pad has a recess of 6 mm diameter and a depth groove of 0.4 mm, the recess has the same area and various shapes. The orifice restrictors were used on the six oil pads. When the bearing operating, lubricant was supplied into the bearing recess through the orifice restrictor. The recesses are symmetrically distributed and liquid resistance of restrictors are equal, all pressure in recesses are equally to ensure the spindle floated, the oil gap between seal surface and spindle also has a liquid resistance to ensure frictionless normal operation. Structural parameters of the hydrostatic thrust bearing are shown in Table 1. The mesh of hydrostatic thrust bearing flow field is generated by the MESH technology in a layered sweep method, and the mesh size between 0.005–0.2 mm. The oil film region is generated by a five-layer tetrahedral mesh with skewness less than 0.35. The oil inlet and recess region were generated by a trigonal and tetrahedral mesh with skewness less than 0.78. The tetrahedral meshing of the oil film region by sweep method helps to compress the oil film region with high quality and makes the iterative process more conducive to convergence. Integral grid number of nodes is 445,668,

number of elements is 386,850, bounding box diagonal is 70.791, average surface area is 14.465 mm², minimum edge length is 2.5e-2 mm.

Figure 1 Model of, (a) hydrostatic thrust bearing (b) recess shape (see online version for colours)

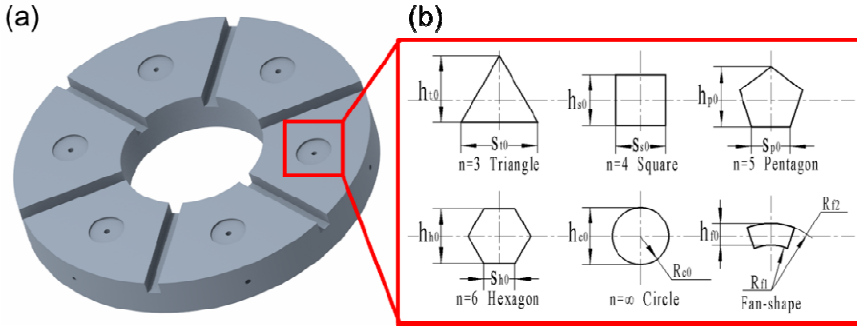


Table 1 Structural parameters of the hydrostatic thrust bearing

Parameter	Symbol	Value	Unit
Number of pads	N	6	-
Outer diameter	D_o	50	mm
Inner diameter	D_i	20	mm
Pad thickness	H	6	mm
Oil film thickness	h	25	μm
Groove width	L_G	2	mm
Groove depth	D_G	2	mm
Area of hydrostatic recess	S_R	19.625	mm ²
Hydrostatic recess depth	H_R	0.35	mm
Restrictor diameter	D_r	0.2	mm
Restrictor length	L_r	1	mm

2.2 Theory of heat flow conservation

In bearing operations, the solid part and the oil film were interacted and ultimately achieved balance, the exchange conditions of displacement, temperature and heat flow are followed. To solve the temperature distribution in the oil film and the orifice restrictor, the energy equation and the heat transfer equation were solved. The temperature distribution governing energy equation is derived (Gang et al., 2022):

$$\rho C_p \left[\frac{\partial T}{\partial t} + \left(u \frac{\partial T}{\partial x} + v \frac{\partial T}{\partial y} + w \frac{\partial T}{\partial z} \right) \right] = \frac{\partial}{\partial y} \left(k \frac{\partial T}{\partial y} \right) + \mu \left[\left(\frac{\partial u}{\partial y} \right)^2 + \left(\frac{\partial w}{\partial y} \right)^2 \right] \quad (1)$$

where ρ is density of lubricants, C_p is constant pressure specific heat capacity, k is thermal conductivity, μ is viscosity of lubricant. For the solid heat transfer equation:

$$\rho_b C_b \frac{\partial T_b}{\partial t} = k_b \left(\frac{\partial^2 T_b}{\partial r_b^2} + \frac{1}{r_b} \frac{\partial T_b}{\partial r_b} + \frac{1}{r_b^2} \frac{\partial^2 T_b}{\partial \theta^2} + \frac{\partial^2 T_b}{\partial Z^2} \right) \quad (2)$$

where T_b is temperature of solid, ρ_b is density of solid, C_b is constant pressure specific heat capacity of solid, k_b is thermal conductivity of solid. To solve the equations (1) and (2), the boundary conditions of temperature field must be determined. Detailed boundary conditions and meshing will be described below.

2.3 Boundary conditions

The equations for fluid flow and heat transfer in hydrostatic thrust bearings were solved by using the CFD method. The bearings operate at speeds of 0–4,000 rpm, the viscous power dissipation of the lubricant is the main source of heat. To solve the equations, the boundary conditions of lubricant contact with the bearing/spindle was assumed as the heat transfer. The heat flow continuous mode was switched on, the heat and temperature continuous in the coupled heat transfer analysis was ensured. The temperature of environment and lubricant were assumed, the approximate boundary heat transfer coefficient was solved by using the Nusselt number N_u in solution. The convective heat transfer between fluid and solid is determined by the G_r and the R_e , which can be derived as follows (Hanna, 2022):

$$G_r = \frac{g\beta L^3 \Delta T}{\nu^2} \quad (3)$$

$$R_e = \frac{\rho u L}{\mu} \quad (4)$$

where g is gravitational acceleration, β is coefficient of volume expansion, ΔT is temperature difference between fluid and solid surface, L is characteristic length of the structure. The following equation of convective heat transfer coefficient is derived:

$$\alpha = \frac{N_u \lambda}{L} \quad (5)$$

where λ is thermal conductivity of fluid. It is clear that the convective heat transfer coefficient is related to N_u from equation (5), which reflects the strength of convective heat transfer. N_u in natural convective heat transfer is determined by G_r and P_r :

$$N_u = 0.59(G_r P_r)^{0.25} \quad (6)$$

where P_r is Prandtl number.

In the bearing flow field, the inlet is setup as a pressure inlet. The supply pressure is set to 1.2 Mpa, and the outlet pressure is set to atmospheric pressure. Temperature of inlet and outlet are all set to environment temperature. The conditions for calculation and initial bearing parameters are listed in Table 2, VG22 lubricant is chosen. In addition, viscosity of lubricant under normal operating conditions is negligible affected by pressure, only the temperature-viscosity effect of the lubricant is considered. The viscosity of lubricant decreases as the temperature increases, the temperature-viscosity relationship of the lubricant is given as follows by the Walter equation:

$$\bar{\mu} = \frac{\mu}{\mu_r} = \exp \left[\bar{\alpha}_1 \left[\frac{1 + \frac{273.15}{T_r}}{\bar{T}_f + \frac{273.15}{T_r}} - 1 \right] \right] \quad (7)$$

where T_r is reference temperature, is dimensionless oil film temperature, μ_r is viscosity of the lubricant at reference temperature. The energy equation was switched on and the viscous shear heating of the oil film was considered in simulation. The physical properties of lubricant were used to derive coefficients for the viscous temperature equation, and applied to the model by setting temperature of the inlet by a UDF.

Table 2 Boundary conditions and bearing parameters

CFD simulation parameter	Value	Unit
Solution methods	Simple	-
Energy equation	On	-
Solution initialisation	Standard initialisation	-
Flow state	Viscous laminar	-
Lubricant	VG22	-
Lubricant density at 15°C	802	Kg/m ³
Dynamic viscosity of oil (40°C)	0.022	Kg/m·s
Dynamic viscosity of oil (100°C)	0.004	Kg/m·s
Supply pressure (relative)	1.2	Mpa
Outlet pressure (relative)	0	Mpa
Environment temperature	27	°C
Flow-solid heat transfer coefficient	35.169	W/(m ² K)
Rotational speed	0–5,000	rpm

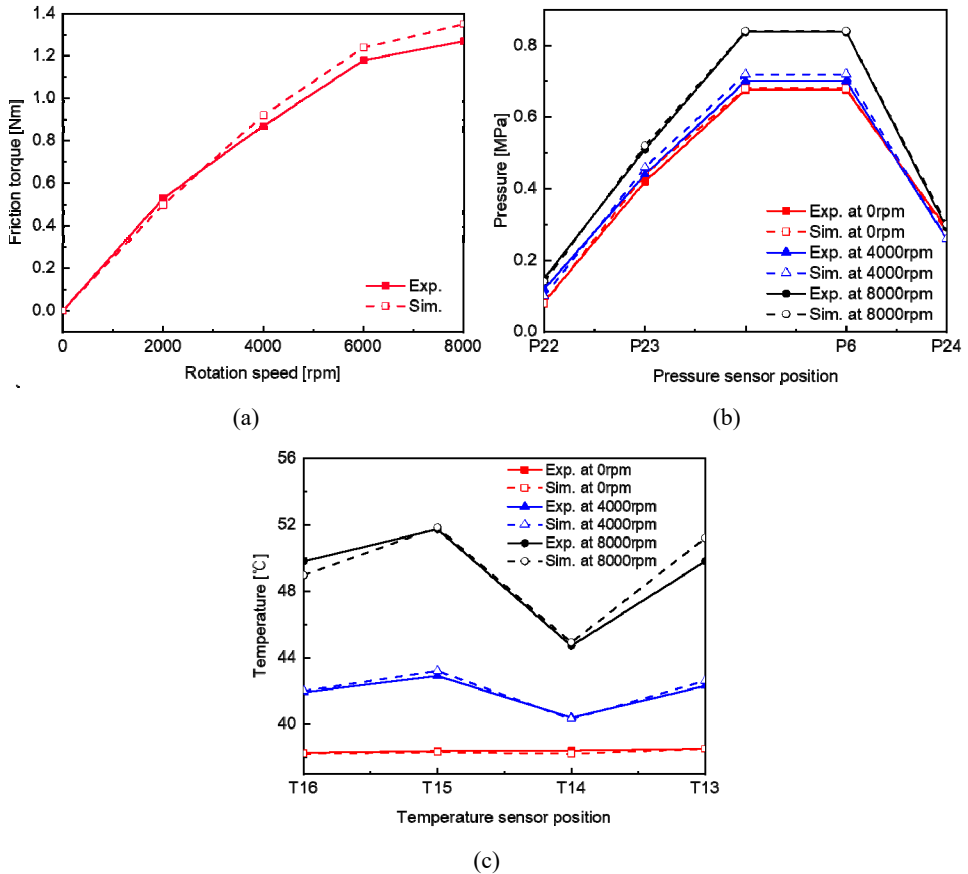
3 Simulation results and discussion

3.1 Validation research

An experiments case was solved using the developed CFD method, and the predictions in current research with the published experiments in Bouyer and Wodtke (2022) were compared. The pressure of lubricant was within 2–2.5 bar, the temperature of lubricant was 313.15 K and the rotational speed was 0–8,000 rpm. Under the five different rotational speeds (0, 2,000, 4,000, 6,000, 8,000 rpm), the extrapolated friction torque of oil film and the published experiments were presented in Figure 2(a). The maximum differences of friction torque between simulation and experimental results were 6.29%. The friction torque increased with the rotation speed, the theoretical simulations fit well with experimental results. Under the three different rotational speeds (0, 4000, 8000 rpm), the pressure variations and temperature rise of oil film compared with the published experiments were presented in Figures 2(b) and 2(c). The maximum differences of pressure variations between simulation and experimental results was 12.7%, and the maximum differences of temperature rise was 5.21%. All maximum difference is less

than 15% between the simulation values and experimental results. Considering the interference of environmental factors, the overall change trend is close to the simulation results. The simulation and experimental results show the rationality of the method.

Figure 2 Comparison of experiments in Bouyer and Wodtke (2022), (a) friction torque (b) pressure (c) temperature (see online version for colours)

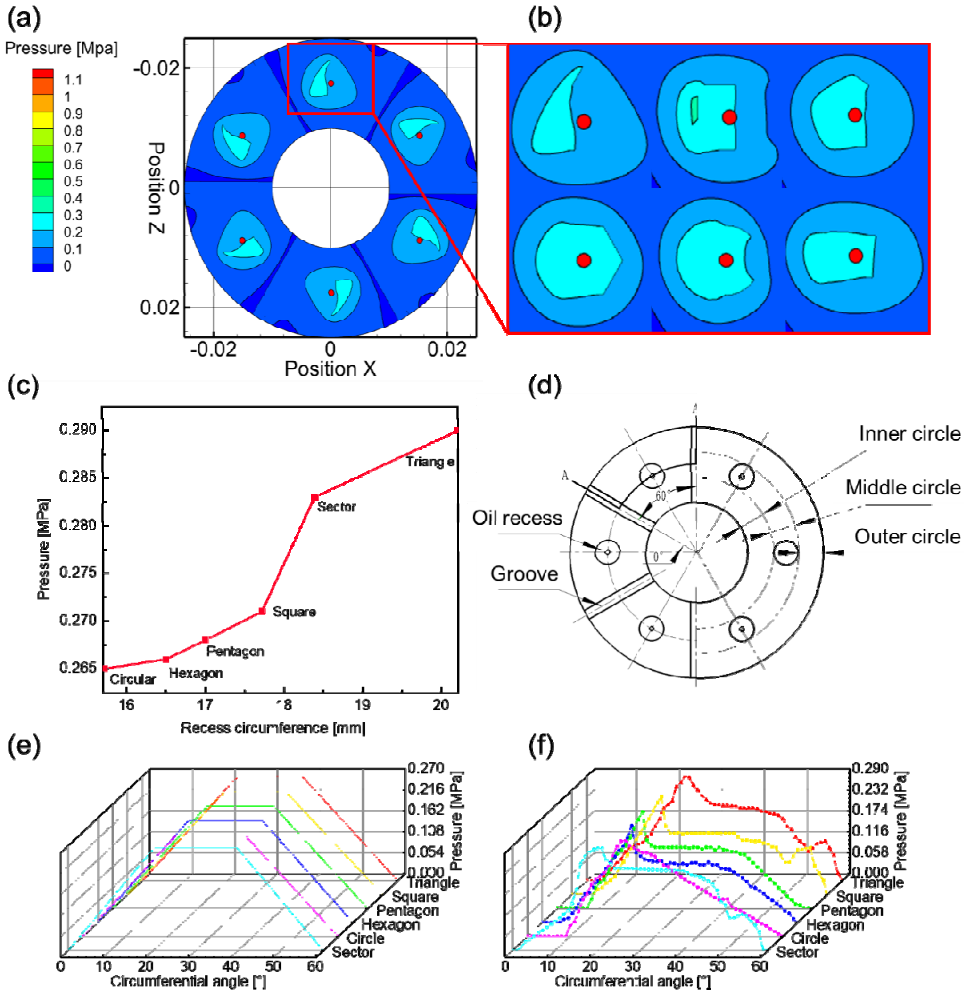


3.2 Pressure distribution

The pressure distribution of oil film as shown in Figure 3. It is under the 5,000 rpm rotation speed, 1.2 Mpa inlet pressure and 25 μm oil film thickness. Figure 3(a) shows a concentration of pressure at inlet under the restrictor action, which the lubricant enters orifice restrictor and recess, the pressure in oil recess area is relatively uniform around 0.3 Mpa. It is noted that pressure of oil recess decreases continuously along the surrounding sealing edge, which reduced to atmospheric pressure at outlet. Pressure distribution on six shapes recessed thrust pad offset to left along the circumference [Figure 3(b)], it is attribute to the direction of rotation speed. The influence of the oil recess shape on the oil film pressure is obviously. After passing through the restrictor, the oil film pressure disperses with reference to the shape of the oil recess. Therefore, the

pressure distribution in circular recess is the most concentrated. The sector recess has the largest range of pressure distribution, due to the sector recess has the longest side length.

Figure 3 (a) Pressure distribution in different recess shapes at 5,000 rpm (b) Magnified view (c) Influence of recess circumference on pressure (d) Section A-A and circle distribution (e) Pressure distribution of section A-A at 0 rpm (f) Pressure distribution of section A-A at 5,000 rpm (see online version for colours)



The variation pressure for different recess shapes is shown in Figure 3(c), with 0.29 Mpa for an equilateral triangle recess, 0.271 Mpa for a square recess, 0.268 Mpa for a regular pentagon recess, 0.266 Mpa for a regular hexagon recess, 0.265 Mpa for a circular recess and 0.283 Mpa for a sector recess. The pressure distribution is positively related to the circumference of the oil recess. At 1.2 Mpa inlet pressure and 5,000 rpm speed, the equilateral triangle recess has the maximum recess pressure and the minimum pressure is circular. It observed the longer circumference recess has the higher average pressure. The pressure gradient for different recess shape are based on the shape with the pressure dropping along the sealing edge from inside to outside. The value of pressure gradient for

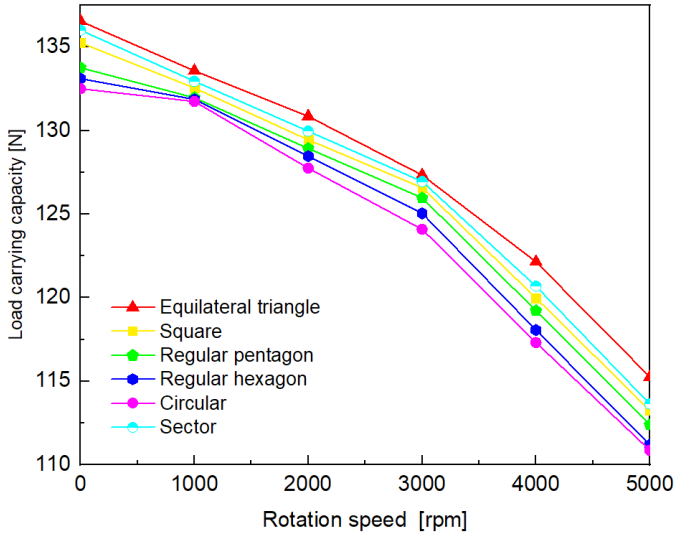
different recess shapes: $P_{triangle} > P_{sector} > P_{square} > P_{pentagon} > P_{hexagon} > P_{circle}$. The pressure distribution curves of section A-A for different types of recess shape at 0 rpm is shown in Figure 3(e), with 0.268 Mpa for equilateral triangle recess, 0.264 Mpa for square recess, 0.263 Mpa for regular pentagon, 0.262 Mpa for regular hexagon recess, 0.260 Mpa for circular recess and 0.266 Mpa for sector recess. It is observed that the pressure distributions of all recess shapes are symmetrical, and pressure section from recess to outlet groove under 0 rpm is liner. The maximum pressure is in equilateral triangle recess, it is not affected by the rotational speed. The pressure distribution of oil film in the A-A section [Figure 3(d)] is deflected to the rotation direction at 5,000 rpm, and it is consistent with the results in Figure 3(b). The maximum pressure rises with the rotation speeds, and pressure gradient in recess was occurred due to the rotational speed. The fluctuations appeared in the pressure curve of triangular, square and sector recess, it causes vibrations in bearing rotation. It has no significant findings in the other three types shape of the recess pressure curve.

3.3 Load carrying capacity

Figure 4 shows the LCC of six different recess shapes obtained for rotation speeds from 0 rpm to 5,000 rpm and 1.2 Mpa inlet pressure and 25 μm oil film thickness. The LCC of equilateral triangle recess is constant at 136.56 N at 0 rpm rotation speed, which is the maximum force. The increase in speed leads to a decrease in the LCC to values of 133.58, 130.86, 127.34, 122.15 and 115.25 N at 1,000, 2,000, 3,000, 4,000 and 5,000 rpm, respectively. It proves the higher rotation speeds, the greater influence of rotation on the LCC, as it is reduced by 15.6% between 0 and 5,000 rpm. However, the pattern of LCC variation for different recess shapes is consistent over the speed variation from 0 to 5,000 rpm, with the maximum LCC at 0 rpm, and accompanied by a decrease in LCC as the rotation speeds increases. In the bearing rotating conditions, the lubricant temperature rise due to internal oil film shear heat is generated. This is due to the viscosity of lubricant when the internal velocity difference will produce shear stress as the speed rises. Therefore, the viscosity becomes smaller when the LCC decreases. The average temperature rise of six different recess shapes at 5,000 rpm exceeds 8.85°C as shown in Figure 7(b), combined with equation (7) the viscosity of lubricant is dropped to 0.017 Kg/m·s. It is indicated that the viscosity of lubricant becomes thinner and the LCC reduced under the influence of high temperature. The variation declines of LCC with different shape of recess, which equilateral triangle recess dropped by 15.6%, square recess dropped by 16.28%, regular pentagon recess dropped by 15.98%, regular hexagon recess dropped by 16.48, circular recess dropped by 16.34%, sector recess dropped by 16.46%. However, influence of the recess shapes is also significant, and cause the variation is 4.83 N between the equilateral triangle recess and circular recess at 4,000 rpm. The following pattern LCC of recess shapes from large to small is observed: $F_{triangle} > F_{sector} > F_{square} > F_{pentagon} > F_{hexagon} > F_{circle}$. It is attributed to the inertial effect of oil film, the circular oil recess will fasten the lubricant outflow, so the LCC is reduced. For the triangle and sector recess, the inertial effect of the oil film will reduce the lubricant outflow so the LCC is greater than the circular oil recess. As the rotational speed increases, the inertial effect increases, and the difference between LCC of six different oil recess bearings also increases. The circumference of recess which equilateral triangle is 20.22 mm, square is 17.72 mm, regular pentagon is 17 mm, regular hexagon is

16.5 mm, circular is 15.7 mm, sector is 18.39 mm. It is clearly that the long circumference of bearing oil recess improves the LCC. The average difference between the maximum and minimum LCC is about 4.12% and the difference independently as the speed increases.

Figure 4 LCC in different recess shapes at 0–5,000 rpm speed (see online version for colours)



3.4 Temperature distribution

The temperature distribution of oil film under 5,000 rpm rotation speed, 1.2 Mpa inlet pressure and 25 μm oil film thickness is shown in Figure 5. To facilitate subsequent part of description, the bearing oil film is divided into three circular parts based on the oil recess as shown in Figure 3(d). The part from the edge of the bearing recess to outer diameter is defined outer circle, from the edge of the bearing oil recess to inner diameter is defined inner circle, and the other circular area formed by inner and outer edges of the oil recess is defined middle circle. The maximum value of oil film temperature is located on the outer diameter of the oil film and the minimum temperature is located on the outer diameter of the bearing at outlet groove in Figure 5(a). There are no significant differences in the temperature distribution of the oil film under different recess shapes, and the concentration of temperature rise is in the outer circle of oil film, followed by the inner circle and middle circle. The temperature rise of the middle circle oil film is the minimum of three parts as observed in Figure 5. It is attribute to the oil recess is exists in the middle circle area, and supplies lubricant to ensure operation constantly. Therefore, the lubricant in this area has the minimum value of the temperature rise. Additionally, for the temperature distribution of oil film, the sector recess is concentrated and the triangle recess more uniform under the same area [Figure 5(b)].

The maximum temperature of the oil film from 0 to 5,000 rpm is shown in Figure 5(d). The maximum temperature of different shaped recesses is exactly the same at 0 rpm, it is no temperature rise. The temperature rises gradually with increasing speed, there is no variation between the different shapes of recesses. It is due to the greatest

linear velocity of outer circle, which the maximum temperature is distributed. The different recess shapes are located in the middle circle independent to the maximum temperature. Figure 5(e) gives the average temperature results of six different recess shapes obtained for rotation speeds from 0 rpm to 5,000 rpm and 1.2 Mpa inlet pressure and 25 μm oil film thickness. The average oil film temperature of different recess shapes is essentially the same at 0 rpm speed, and there is no temperature rise in the oil film. The temperature rise is mainly from heat exchange between lubricant and bearing due to no friction in the oil film, and the average temperature of six recess shapes as the same as the ambient temperature. The variations in temperature rise between different recess shapes appeared at the speed increases, and the higher speed the more significant difference. The difference of average temperature between sector recess and triangle is 2.3% at 5,000 rpm. The order average temperature is observed: $T_{\text{sector}} > T_{\text{square}} > T_{\text{hexagon}} > T_{\text{circle}} > T_{\text{pentagon}} > T_{\text{triangle}}$. Combined with Figures 1(b) and 3(d), the six different shapes of the bearing circle distribution have different widths. The width of equilateral triangle recess h_{t0} is 5.837 mm, the width of square recess h_{s0} is 4.43 mm, the width of regular pentagon h_{p0} is 5.23 mm, the width of regular hexagon recess h_{h0} is 4.76 mm, the width of circular recess h_{c0} is 5 mm, the width of sector recess h_{f0} is 3.2 mm. Therefore, the average temperature of the oil film is inversely proportional to the width of middle circle, the smaller width of the bearing, the lower the average temperature rise is appearance. It is attributed to the fact that the temperature rise of the middle circle is lower than the outer and inner circle, due to the constant flow of lubricant into the bearing during rotation.

4 Experimental testing

The hydrostatic thrust bearing test rig used for the experiment as shown in Figure 6. A hydraulic station with a precision of $\pm 0.5\%$ was used to supply oil to the thrust bearing. The test rig composed of screw load mechanism, test cell, precision turntable (ADR110-A98, AKRIBIS, Singapore), thrust plate, bearings and sensors. The precision turntable is driven by its own drive, and the standard axial/radial run-out is 0.015 μm . The hydrostatic thrust bearing is loaded by a screw load mechanism, and controlled by a force sensor. The applied load range is 50–500 N. Schematic of the test cell as shown in Figure 6(a). A spherical dimple is set on the connection plate to keep self-alignment when the applied load.

The tested hydrostatic thrust bearing is shown in Figure 6(b). In this article, the sector oil recess is chosen to measure the LCC and temperature at different speeds. The restrictor is machined externally and then installed. To measure the temperature of oil film at different locations, five temperature sensors are set. The holes were punched in the bearing surface and the platinum resistors were used as temperature sensors were placed. The pressure sensors are connected to the oil recesses by using an external hose to measure the pressure in each recess. To ensure uniform distribution of the oil film, the pressure in six recesses is equalised by controlling the spherical dimple on the connection plate. The load was applied to the bearing by force sensor, the measuring range and resolution were 500 N and 0.1 N respectively. A laser displacement sensor (Keyence LK-H020, Measuring Instruments, Japan) was used to auxiliary measurement of axial displacement, with a measuring range and repetition accuracy are 20 mm and 0.02 μm respectively. The oil supply pressure in the experiment was 12 bars. To exclude the

factors affecting the experiment such as machining errors, installation errors and fluctuations in oil supply pressure, the experimental results were repeated five times and averaged.

The maximum speed of the turntable is 1,500 rpm. To ensure the results and the safety of the experiment, the relatively high speed of 1,000 rpm was selected in the experiment. The CFD simulation method was used to analyse the LCC and temperature at 1,000 rpm rotational speeds. Under the same operating conditions, if the experimental results are the same as the simulation, the CFD simulation method is validated. Figures 6(c) and 6(d) show the results of experimental and CFD simulation on the sector oil recess thrust bearing, the oil recess pressure and temperature were compared respectively. The maximum difference in data is within 5%, for the errors between experimental and calculated, it is acceptable. The CFD simulation results are agreement with the experimental results, the validity of the CFD simulation method and the corresponding numerical results were verified.

5 Conclusions

In this article, an effective CFD simulation method is used to investigate the influences on multi-recess thrust bearings of six different shapes. A validation research based on published experiments was conducted, the differences of friction torque, pressure variations and temperature rise are all less than 12.7%. The pressure distribution, temperature and LCC of oil film were simulated at different speeds. Finally, the experiments on the hydrostatic thrust bearing test rig were carried out to validating the CFD methods. Following conclusions have been observed:

- 1 The pressure distribution of oil recess increases with the recess circumference, when the area of recess is certain. The maximum recess pressure of the six shapes is equilateral triangle recess and the minimum pressure is circular, which have a 9% difference between them.
- 2 The LCC also increases with the recess circumference at same speed. The maximum of the six shapes is equilateral triangle recess and the minimum pressure is circular, which have a 4.12% variation. The LCC of all bearings decreases with the increase of rotation speed, the maximum decreased of the same bearing by 16.46% when the speed from 0 to 5,000 rpm at same operating conditions.
- 3 The different shapes of recess have no significant difference on temperature distribution and maximum temperature of the oil film, while have an effect on the average temperature. The temperature rises of different recess shapes from low to high is in the following order when the speed increases: $T_{sector} > T_{square} > T_{hexagon} > T_{circle} > T_{pentagon} > T_{triangle}$, and the average temperature rise of oil film is inversely proportional to the width of the bearing middle circle. The variation in average temperature rise between different recess shapes occurs as the speed increases, with a 2.3% difference between the sector and the equilateral triangle at 5,000 rpm.
- 4 The maximum difference between the experimental and simulation results is within 5%. The validity of the CFD simulation method and the corresponding numerical results were verified.

Figure 5 (a) Temperature distribution in different recess shapes (b) Magnified view (c) Temperature distribution in different speed between 1,000–5,000 rpm (d) Maximum temperature (e) Average temperature (f) Influence of middle circle width on average temperature of oil film (see online version for colours)

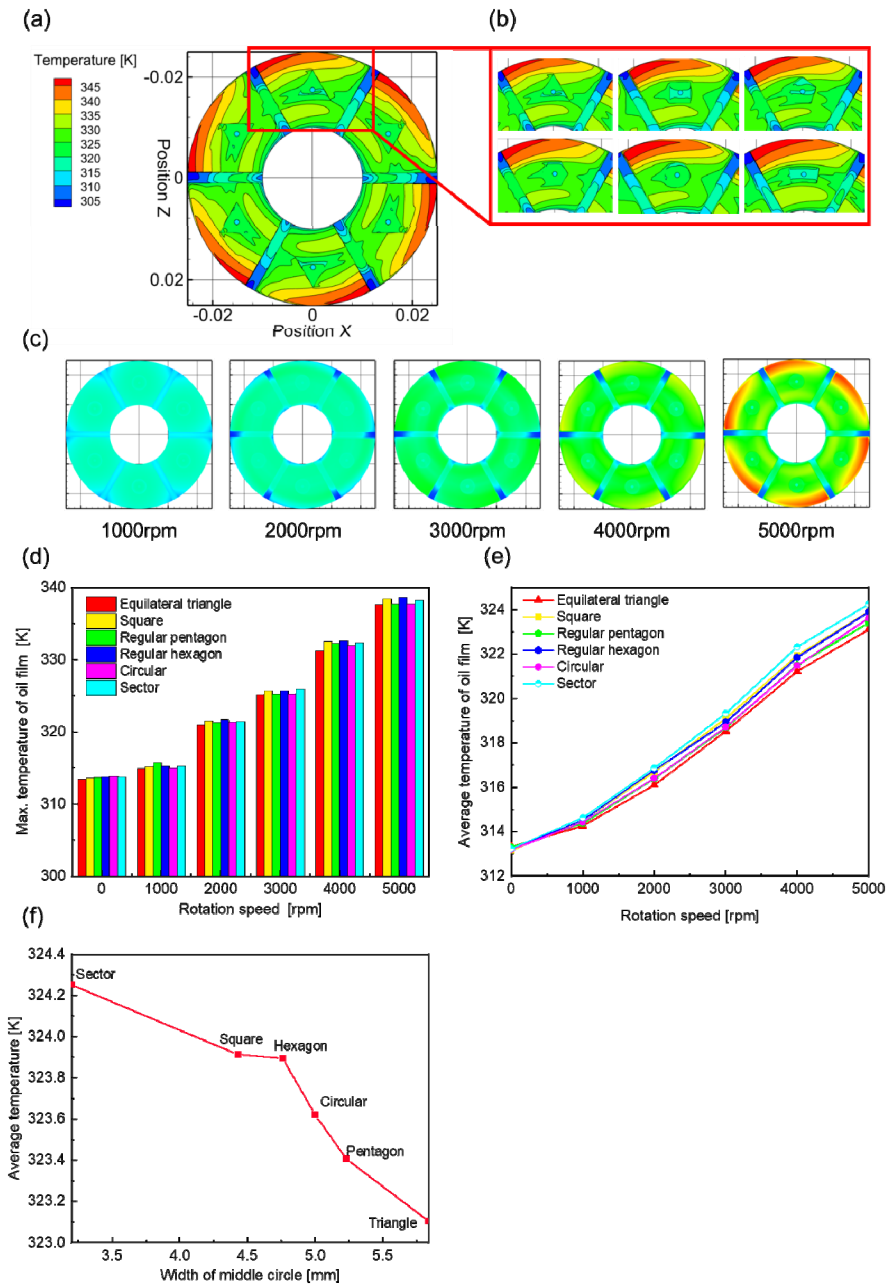
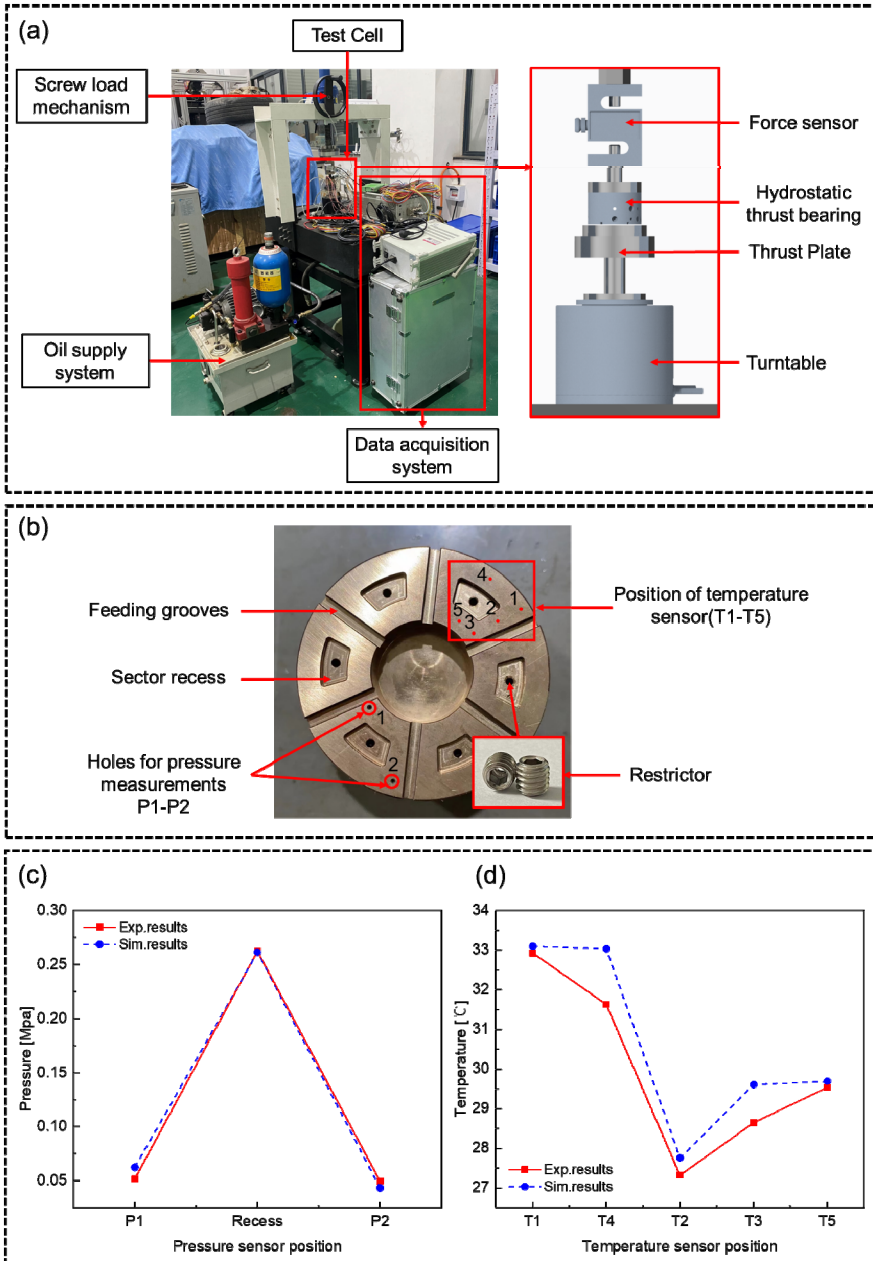


Figure 6 (a) Hydrostatic thrust bearing test rig (b) Construction of the tested bearing (c) (d) Comparisons of CFD simulation and experimental result (see online version for colours)



The results of CFD simulation method are consistent with the experiments, indicating the validity of the theoretical analysis in this paper. However, the study of the oil recess structure is limited to two-dimensional structure, and the depth of recess and the shape of inner edge are not involved. This will be the focus of our next research.

Credit author statement

Minghui Guo: conceptualisation, methodology and writing-original draft preparation; Zhuxin Tian: supervision and project administration; Xiaolin Feng: formal analysis; Yu Huang: resources and investigation; Guojun Zhang: supervision; and Youmin Rong: writing-reviewing and editing.

Acknowledgements

This research is supported by National Key R&D Program of China (No. 2020YFB2007600) and National Natural Science Foundation of China (No. 51875223).

References

- Bouyer, J.M. and Wodtke, M.F. (2022) 'Experimental research on a hydrodynamic thrust bearing with hydrostatic lift pockets: influence of lubrication modes on bearing performance', *Tribology International*, Vol. 165, No. 1, p.107253.
- Bouzidane, A. and Thomas, M. (2007) 'Equivalent stiffness and damping investigation of a hydrostatic journal bearing', *Tribol. Trans.*, Vol. 50, No. 2, pp.257–267.
- Dong, W., Li, B. and Guo, W. (2020) 'Prediction of different design conditions on comprehensive performance of hydrostatic slide and experimental verification', *Int. J. Adv. Manuf. Tech.*, Vol. 107, No. 3, pp.535–547.
- Dzodzo, M., Braun, M.J. and Hendricks, R.C. (1996) 'Pressure and flow characteristics in a shallow hydrostatic pocket with rounded pocket/land joints', *Tribol. Int.*, Vol. 29, No. 4, pp.69–76.
- Gang, L., Huang, G., Yuan, H., Xia, S. and Tan, W. (2022) 'Analysis and optimisation of impact wear of diesel engine needle valve assembly', *Int. J. Hydromechatronics*, Vol. 5, No. 1, pp.80–91.
- Hanna, J. (2022) 'Accurate computational modelling for impacts of microcapsule size and interfacial fracture properties on the fracture of self-healing concrete', *Int. J. Hydromechatronics*, Vol. 5, No. 4, pp.397–415.
- Kozdera, M. and Drbáková, S. (2013) 'Numerical modelling of the flow in the annular multi-recess hydrostatic thrust bearing using CFD methods', *EPJ Web of Conferences*, Vol. 45, No. 2, p.1051.
- Kumar, V. and Sharma, S.C. (2017) 'Combined influence of couple stress lubricant, recess geometry and method of compensation on the performance of hydrostatic circular thrust pad bearing', *Proc. IMechE Part J: J. Engineering Tribology*, Vol. 231, No. 6, pp.716–733.
- Kumar, V. and Sharma, S.C. (2019) 'Magneto-hydrostatic lubrication of thrust bearings considering different configurations of recess', *Industrial Lubri. & Tribol.*, Vol. 71, No. 7, pp.915–923.
- Kumar, V., Shah, V.A. and Narwat, K. (2020) 'Dynamic performance of an externally pressurized porous thrust bearing employing different pocket shape', *Tribology Online*, Vol. 15, No. 5, pp.380–387.
- Li, J., Sui, T., Dong, X., Gu, F., Su, N., Liu, J. and Xu, C. (2022) 'Large eddy simulation studies of two-phase flow characteristics in the abrasive flow machining of complex flow ways with a cross-section of cycloidal lobes', *Int. J. Hydromechatronics*, Vol. 5, No. 2, pp.136–166.

- Liu, B.K. and Lu, W.Z. (2022) 'Surrogate models in machine learning for computational stochastic multi-scale modelling in composite materials design', *Int. J. Hydromechatronics*, Vol. 5, No. 4, pp.336–365.
- Liu, Z.R. and Yang, W.Y. (2022) 'Theoretical analysis and numerical study on a flexible piezoelectric wave energy converter', *Int. J. Hydromechatronics*, Vol. 5, No. 4, pp.292–310.
- Michalec, M., Svoboda, P. and Krupka, I. (2021) 'A review of the design and optimization of large-scale hydrostatic bearing systems', *Engineering Sci. &Tech.*, Vol. 24, No. 4, pp.936–958.
- Saurabh, K., Yadav, N. and Sharma, S.C. (2014) 'Performance of hydrostatic tilted thrust pad bearings of various recess shapes operating with non-Newtonian lubricant', *Finite Elements in Analysis & Design*, Vol. 87, No.2, pp.43–55.
- Shaaban, A.M. (2022) 'A review article: isogeometric boundary element analysis in engineering applications', *Int. J. Hydromechatronics*, Vol. 5, No. 4, pp.366–396.
- Sharma, S.C., Jain, S.C. and Bharuka, D.K. (2002) 'Influence of recess shape on the performance of a capillary compensated circular thrust pad hydrostatic bearing', *Tribology International*, Vol. 35, No. 6, pp.347–356.
- Shen, F., Chen, C.L. and Liu, Z.M. (2014) 'Effect of pocket geometry on the performance of a circular thrust pad hydrostatic bearing in machine tools', *Tribol. Trans.*, Vol. 57, No. 4, pp.700–714.
- Singh, N., Sharma, S.C., Jain, S.C. and Reddy, S.S. (2004) 'Performance of membrane compensated multirecess hydrostatic/hybrid flexible journal bearing system considering various recess shapes', *Tribol. Int.*, Vol. 37, No. 2, pp.11–24.
- Untaroiu, A. and Fu, G. (2017) 'Effect of recess shape on the performance of a high-speed hybrid journal bearing', *J. Engineering for Gas Turbines & Power*, Vol. 139, No. 11, p.112501.
- Xu, X.Q., Shao, J.P., Yang, X.D., Zhang, Y.Q., Yu, X.D. and Gao, B.W. (2013) 'Simulation on multi-oil-cavity and multi-oil-pad hydrostatic bearings', *Applied Mechanics & Materials*, Vol. 274, pp.274–277.
- Xue, B., Wei, C., Hu, J.B. (2018) 'Research on effects of groove shape optimization on cavitation and lubricating characteristics for microgroove rotary seal', *Tribol. Trans.*, Vol. 61, No. 3, pp.569–584.
- Yacout, A.W. (2007) 'The surfaces roughness effect on the hydrostatic thrust spherical bearings performance (part 3 of 5, recessed clearance type of bearings)', *ASME Int. Mech. Eng. Congr. Expo. Proc.*, pp.431–447.
- Yacout, A.W., Ismaeel, A.S. and Kassab, S.Z. (2006) 'The surface roughness effect on the hydrostatic thrust spherical bearing performance (part 2 of 5, clearance type of bearings)', *Am. Soc. Mech. Eng. Tribol. Div. TRIB*, pp.77–91.
- Yu, M.B., Yu, X.D. and Zheng, X.H. (2019) 'Influence of recess shape on comprehensive lubrication performance of high speed and heavy load hydrostatic thrust bearing', *Industrial Lubrication & Tribology*, Vol. 71, No. 2, pp.301–308.
- Yu, X.D., Sun, D.D., Meng, X.L., Wu, X.G., Sui, J.L., Zhang, Y.Q. and Wang, W.S. (2015) 'Velocity characteristic on oil film thickness of multi-pad hydrostatic thrust bearing with circular recess', *J. Computational & Theoretical Nanoscience*, Vol. 12, No. 10, pp.3155–3161.
- Zhang, Y.Q., Yang, X.D. and Li, H.M. (2010) 'Research on influence of cavity depth on load capacity of heavy hydrostatic bearing in variable viscosity condition', *Advanced Materials Research*, Vols. 129–131, pp.1181–1185.
- Zhang, Y.Q., Zhang, Z.Q. and Feng, Y.N. (2018) 'Lubrication characteristics of double rectangular cavity hydrostatic bearing at high speed', *Tribology*, Vol. 38, No. 5, pp.609–618.